

Resummation of the transverse-energy distribution in Higgs boson production at the Large Hadron Collider

Massimiliano Grazzini^{a*}, Andreas Papaefstathiou^a, Jennifer M. Smillie^b and Bryan R. Webber^c

^a*Physik Institut, Universität Zürich, Switzerland*

^b*Higgs Centre for Theoretical Physics, University of Edinburgh, UK*

^c*Cavendish Laboratory, J.J. Thomson Avenue, Cambridge, UK*

E-mail: grazzini@physik.uzh.ch, andreasp@physik.uzh.ch, j.m.smillie@ed.ac.uk,
webber@hep.phy.cam.ac.uk

ABSTRACT: We compute the resummed hadronic transverse-energy (E_T) distribution due to initial-state QCD radiation in the production of a Standard Model Higgs boson of mass 126 GeV by gluon fusion at the Large Hadron Collider, with matching to next-to-leading order calculations at large E_T . Effects of hadronization, underlying event and limited detector acceptance are estimated using `aMC@NLO` with the `Herwig++` and `Pythia8` event generators.

KEYWORDS: Higgs boson, Hadronic Colliders, QCD Phenomenology.

*On leave of absence from INFN, Sezione di Firenze, Sesto Fiorentino, Florence, Italy.

Contents

1. Introduction	1
2. Resummation of logarithmically enhanced terms	3
2.1 Evaluation of the exponent	5
3. Matching to fixed order	8
3.1 Expansion of the resummed prediction	8
3.2 Matching to NLO	11
3.3 Results	12
4. Monte Carlo studies	14
4.1 E_T at parton level	15
4.2 E_T at hadron level	17
4.3 Inclusion of the underlying event	17
5. Conclusions	19
A. Proof of an identity	20
B. Dispersion relations	20
C. Comparison with transverse-momentum resummation	22
D. Alternative Monte Carlo results	23

1. Introduction

The new particle discovered recently by the ATLAS [1] and CMS [2] Collaborations at the LHC looks very much like the Higgs boson of the Standard Model, although its properties remain to be fully explored. For this exploration, detailed predictions of the expected characteristics of Higgs production within the Standard Model will be essential, in order to optimize signal to background ratios and to search for any signs of new physics. One such characteristic is the amount and distribution of initial-state QCD radiation, which is predicted to be exceptionally high in production by gluon fusion and exceptionally low in vector boson fusion. A thorough understanding of initial-state radiation is therefore essential for the separation of these production mechanisms.

In the present paper we study the distribution of the total amount of transverse energy (E_T) emitted in Standard Model Higgs boson production by gluon fusion at the LHC.

Results are presented at next-to-leading order (NLO) in QCD perturbation theory and also resummed to all orders in the QCD coupling α_S . The resummation applies to leading, next-to-leading and some important next-to-next-to-leading logarithms of E_T/Q ((N)NLL) where Q is the hard process scale, taken to be the Higgs mass m_H . Thus it improves the treatment of the small- E_T region, where the fixed-order prediction diverges whereas the actual distribution must tend to zero as $E_T \rightarrow 0$. By matching the resummed prediction to the NLO result valid at large E_T , we provide a uniform description from the low- E_T to the high- E_T region.

Our approach follows on from Ref. [3], based in turn on the early work on E_T resummation in vector-boson production [4–6] and closely related to the resummation of transverse momentum in vector-boson [7–10] and Higgs production [11–14].¹ We make a number of improvements relative to Ref. [3], including:

- Predictions for the experimentally relevant Higgs mass of 126 GeV, at centre-of-mass energies $\sqrt{s} = 8$ and 14 TeV;
- Fixed-order predictions to NLO, i.e. $\mathcal{O}(\alpha_S^4)$.
- Expansion of the E_T resummation formula to NLO, and demonstration that to this order the structure of the logarithmic terms is consistent with the fixed-order prediction;
- Matching of the resummed and NLO predictions across the whole range of E_T ;
- A constraint on the perturbative unitarity of the prediction, using the method of Ref. [11], which reduces the impact of logarithmic terms in the large- E_T region;
- Studies of the effects of renormalization scale variation and unknown higher-order terms;
- Monte Carlo studies of the effects of hadron-level cuts on pseudorapidity and transverse momentum, with fixed-order matching to parton showers using `aMC@NLO` interfaced to `Herwig++` and `Pythia8`.

The paper is organized as follows. In Sec. 2, we review the resummation procedure and then describe the necessary modifications to implement the unitarity condition mentioned above. This involves some changes in the formalism and the evaluation of new integrals in this prescription. In Sec. 3, we expand our resummed result to next-to-leading order in order to match our results to the fixed-order prediction at this accuracy. This renders our predictions positive throughout the E_T -range. In Sec. 4, we investigate the E_T distribution further through Monte Carlo studies. We first reweight Monte Carlo results to our analytic distribution and then investigate the impact of hadronisation and underlying event. We end the main text in Sec. 5 with conclusions and discussion. A number of appendices then contain supplementary results.

¹The resummation of the jet-veto p_T distribution has been considered in Refs. [15–19].

2. Resummation of logarithmically enhanced terms

Here we summarize the results of Ref. [3] as applied to Higgs boson production. The resummed component of the transverse-energy distribution in the process $h_1 h_2 \rightarrow H X$ at scale Q has the form

$$\left[\frac{d\sigma_H}{dQ^2 dE_T} \right]_{\text{res.}} = \frac{1}{2\pi} \sum_{a,b} \int_0^1 dx_1 \int_0^1 dx_2 \int_{-\infty}^{+\infty} d\tau e^{-i\tau E_T} f_{a/h_1}(x_1, \mu) f_{b/h_2}(x_2, \mu) \cdot W_{ab}^H(x_1 x_2 s; Q, \tau, \mu) \quad (2.1)$$

where $f_{a/h}(x, \mu)$ is the parton distribution function (PDF) of parton a in hadron h at factorization scale μ , taken to be the same as the renormalization scale here (we illustrate the impact of varying this scale in Sec. 3). In what follows we use the $\overline{\text{MS}}$ renormalization scheme. To take into account the constraint that the transverse energies of the emitted partons should sum to E_T , the resummation procedure is carried out in the domain that is Fourier conjugate to E_T . The transverse-energy distribution (2.1) is thus obtained by performing the inverse Fourier transformation with respect to the ‘‘transverse time’’, τ . The factor W_{ab}^H is the perturbative and process-dependent partonic cross section that embodies the all-order resummation of the large logarithms $\ln(Q\tau)$. Since τ is conjugate to E_T , the limit $E_T \ll Q$ corresponds to $Q\tau \gg 1$.

As in the case of transverse-momentum resummation [20], the resummed partonic cross section can be written in the following form:

$$W_{ab}^H(s; Q, \tau, \mu) = \int_0^1 dz_1 \int_0^1 dz_2 C_{ga}(\alpha_S(\mu), z_1; \tau, \mu) C_{gb}(\alpha_S(\mu), z_2; \tau, \mu) \delta(Q^2 - z_1 z_2 s) \cdot \sigma_{gg}^H(Q, \alpha_S(Q)) S_g(Q, \tau) \quad (2.2)$$

Here σ_{gg}^H is the cross section for the partonic subprocess of gluon fusion, $gg \rightarrow H$, through a massive-quark loop:

$$\sigma_{gg}^H(Q, \alpha_S(Q)) = \delta(Q^2 - m_H^2) \sigma_0^H, \quad (2.3)$$

where in the limit of infinite quark mass

$$\sigma_0^H = \frac{\alpha_S^2(m_H) G_F m_H^2}{288\pi\sqrt{2}}. \quad (2.4)$$

$S_g(Q, \tau)$ is the appropriate gluon form factor, which in the case of E_T resummation takes the form [5, 6]

$$S_g(Q, \tau) = \exp \left\{ -2 \int_0^Q \frac{dq}{q} \left[2A_g(\alpha_S(q)) \ln \frac{Q}{q} + B_g(\alpha_S(q)) \right] (1 - e^{iq\tau}) \right\}. \quad (2.5)$$

The functions $A_g(\alpha_S)$, $B_g(\alpha_S)$, as well as the coefficient functions C_{ga} in Eq. (2.2), contain no $\ln(Q\tau)$ terms and are perturbatively computable as power expansions with constant

coefficients:

$$A_g(\alpha_S) = \sum_{n=1}^{\infty} \left(\frac{\alpha_S}{\pi}\right)^n A_g^{(n)} , \quad (2.6)$$

$$B_g(\alpha_S) = \sum_{n=1}^{\infty} \left(\frac{\alpha_S}{\pi}\right)^n B_g^{(n)} , \quad (2.7)$$

$$C_{ga}(\alpha_S, z) = \delta_{ga} \delta(1-z) + \sum_{n=1}^{\infty} \left(\frac{\alpha_S}{\pi}\right)^n C_{ga}^{(n)}(z) . \quad (2.8)$$

Thus a calculation to NLO in α_S involves the coefficients $A_g^{(1)}$, $A_g^{(2)}$, $B_g^{(1)}$, $B_g^{(2)}$ and $C_{ga}^{(1)}$. The coefficients $A_g^{(1)}$, $A_g^{(2)}$, $B_g^{(1)}$ and $C_{ga}^{(1)}$ read [21, 22]

$$\begin{aligned} A_g^{(1)} &= C_A , & A_g^{(2)} &= \frac{1}{6} C_A \left[C_A \left(\frac{67}{6} - \frac{\pi^2}{2} \right) - \frac{5}{3} n_f \right] , & B_g^{(1)} &= -\frac{1}{6} (11 C_A - 2 n_f) , \\ C_{gg}^{(1)}(z) &= \frac{1}{4} \left[C_A \left(2 - \frac{\pi^2}{3} \right) + 5 + 4\pi^2 \right] \delta(1-z) \equiv c_g^{(1)} \delta(1-z) , \\ C_{gq}^{(1)}(z) &= C_{g\bar{q}}^{(1)}(z) = \frac{1}{2} C_F z . \end{aligned} \quad (2.9)$$

The coefficient $B_g^{(2)}$ for the Higgs transverse-momentum spectrum is [23, 24]

$$\bar{B}_g^{(2)} = C_A^2 \left(\frac{23}{24} + \frac{11}{18} \pi^2 - \frac{3}{2} \zeta_3 \right) + \frac{1}{2} C_F n_f - C_A n_f \left(\frac{1}{12} + \frac{\pi^2}{9} \right) - \frac{11}{8} C_F C_A . \quad (2.10)$$

However, the value of the coefficient $B_g^{(2)}$ for the transverse energy in Higgs production could be different². In Sec. 3, we will perform a fit to the fixed-order NLO result at small transverse energy, with this coefficient as a free parameter.

Returning to Eq. (2.1), we may recast it in a form with a real integrand as

$$\begin{aligned} \left[\frac{d\sigma_H}{dQ^2 dE_T} \right]_{\text{res.}} &= \frac{1}{\pi s} \int_0^\infty d\tau e^{-F_g^{(R)}(Q, \tau)} \left[R_g^{(R)}(s; Q, \tau) \cos\{F_g^{(I)}(Q, \tau) + \tau E_T\} \right. \\ &\quad \left. + R_g^{(I)}(s; Q, \tau) \sin\{F_g^{(I)}(Q, \tau) + \tau E_T\} \right] \sigma_{gg}^H(Q, \alpha_S(Q)) \end{aligned} \quad (2.11)$$

where $F_g^{(R)}$ and $F_g^{(I)}$ are the real and imaginary parts of

$$F_g(Q, \tau) = 2 \int_0^Q \frac{dq}{q} \left[2A_g(\alpha_S(q)) \ln \frac{Q}{q} + B_g(\alpha_S(q)) \right] (1 - e^{iq\tau}) . \quad (2.12)$$

As explained in [3], the coefficient functions in Eq. (2.2) contain logarithms of $\mu\tau$, which are eliminated by the choice of factorization scale $\mu_F = \tau_0/\tau$, where $\tau_0 = \exp(-\gamma_E) = 0.56146\dots$, γ_E being the Euler-Mascheroni constant. The resulting expressions for $R_g^{(R, I)}$

²We are grateful to Jon Walsh for a useful discussion on this point.

are

$$\begin{aligned}
R_g^{(R)}(\xi, \tau) &= \int_{\xi}^1 \frac{dx_1}{x_1} \left\{ f_{g/h_1}(x_1) f_{g/h_2} \left(\frac{\xi}{x_1} \right) \left(1 + \frac{\alpha_S}{\pi} 2c_g^{(1)} \right) \right. \\
&\quad \left. + \frac{\alpha_S}{\pi} \int_{\xi/x_1}^1 \frac{dz}{z} \left[f_{g/h_1}(x_1) f_{s/h_2} \left(\frac{\xi}{zx_1} \right) + f_{s/h_1}(x_1) f_{g/h_2} \left(\frac{\xi}{zx_1} \right) \right] \frac{1}{2} C_F z \right\}, \\
R_g^{(I)}(\xi, \tau) &= \frac{\alpha_S}{2} \int_{\xi}^1 \frac{dx_1}{x_1} \int_0^1 \frac{dz}{z} \left\{ 2f_{g/h_1}(x_1) f_{g/h_2} \left(\frac{\xi}{zx_1} \right) P_{gg}(z) \right. \\
&\quad \left. + \left[f_{g/h_1}(x_1) f_{s/h_2} \left(\frac{\xi}{zx_1} \right) + f_{s/h_1}(x_1) f_{g/h_2} \left(\frac{\xi}{zx_1} \right) \right] P_{gq}(z) \right\} \\
&= \frac{\alpha_S}{2} \int_{\xi}^1 \frac{dx_1}{x_1} \left\{ 2f_{g/h_1}(x_1) f_{g/h_2} \left(\frac{\xi}{x_1} \right) \left[2C_A \ln \left(1 - \frac{\xi}{x_1} \right) + \frac{1}{6} (11C_A - 2n_f) \right] \right. \\
&\quad \left. + \int_{\xi/x_1}^1 \frac{dz}{z} \left[4C_A f_{g/h_1}(x_1) \left\{ f_{g/h_2} \left(\frac{\xi}{zx_1} \right) \left[\frac{z}{1-z} + \frac{1-z}{z} + z(1-z) \right] - f_{g/h_2} \left(\frac{\xi}{x_1} \right) \frac{z}{1-z} \right\} \right. \right. \\
&\quad \left. \left. + \left\{ f_{g/h_1}(x_1) f_{s/h_2} \left(\frac{\xi}{zx_1} \right) + f_{s/h_1}(x_1) f_{g/h_2} \left(\frac{\xi}{zx_1} \right) \right\} C_F \frac{1+(1-z)^2}{z} \right] \right\}, \tag{2.13}
\end{aligned}$$

where $f_s = \sum_q (f_q + f_{\bar{q}})$ and all PDFs and coefficient functions are understood to be evaluated at scale $\mu_F = \tau_0/\tau$. We have defined $\xi = Q^2/s$ for convenience.

2.1 Evaluation of the exponent

We now seek to evaluate the exponent of the form factor, (2.12), analytically. We will use the method of Ref. [11] where the analogous calculation was performed for transverse-momentum resummation. In the notation of that paper, we have, for a renormalization scale μ_R ,

$$G_g(a_R, L) \equiv -2 \int_{b_0/b}^Q \frac{dq}{q} \left[2A_g(\alpha_S(q)) \ln \frac{Q}{q} + B_g(\alpha_S(q)) \right] = L g_1(Y) + g_2(Y) + a_R g_3(Y) + \dots \tag{2.14}$$

where $a_R = \alpha_S(\mu_R)/\pi$, $L = 2 \ln(Qb/b_0)$, $Y = \beta_0 a_R L$ and $\beta_0 = (11C_A - 2n_f)/12$ is the lowest-order coefficients of the beta function:

$$\frac{d \ln a_R}{d \ln \mu_R^2} = \beta(a_R) = - \sum_{n=0}^{\infty} \beta_n a_R^{n+1}. \tag{2.15}$$

The term $L g_1(Y)$ collects the LL contributions $\alpha_S^n L^{n+1}$, the function g_2 resums the NLL contributions $\alpha_S^n L^n$, the function g_3 controls the NNLL terms $\alpha_S^n L^{n-1}$, and so forth. We will give the explicit form of the g_i functions below. We can therefore deduce that in general

$$-2 \int_{Q_0}^Q \frac{dq}{q} \left[2A_g(\alpha_S(q)) \ln \frac{Q}{q} + B_g(\alpha_S(q)) \right] = 2\lambda g_1(y) + g_2(y) + a_R g_3(y) + \dots \tag{2.16}$$

where now

$$y \equiv 2\beta_0 a_R \lambda \quad \text{and} \quad \lambda \equiv \ln(Q/Q_0). \quad (2.17)$$

Now by expressing $\alpha_S(q)$ in terms of $\alpha_S(Q)$ and relating this in turn to $\alpha_S(\mu_R)$, we can write the integrand in (2.16) as a function of $\ln(Q/q)$, and then use the result

$$\int_{Q_0}^Q \frac{dq}{q} f\left(\ln \frac{Q}{q}\right) = f\left(\frac{d}{du}\right) \frac{1}{u} \left(e^{\lambda u} - 1\right) \Big|_{u=0}, \quad (2.18)$$

which is easily seen by expanding the exponential. This allows one to calculate the g_i functions explicitly. They are given by [11, 25, 26]:

$$\begin{aligned} g_1(y) &= \frac{A_g^{(1)}}{\beta_0 y} (y + \ln(1-y)), \\ g_2(y) &= \frac{B_g^{(1)}}{\beta_0} \ln(1-y) - \frac{A_g^{(2)}}{\beta_0^2} \left(\frac{y}{1-y} + \ln(1-y)\right) \\ &\quad + \frac{A_g^{(1)} \beta_1}{\beta_0^3} \left(\frac{1}{2} \ln^2(1-y) + \frac{y + \ln(1-y)}{1-y}\right) + \frac{A_g^{(1)}}{\beta_0} \left(\frac{y}{1-y} + \ln(1-y)\right) \ln\left(\frac{Q^2}{\mu_R^2}\right), \\ g_3(y) &= -\frac{A_g^{(3)}}{2\beta_0^2} \left(\frac{y}{1-y}\right)^2 - \frac{B_g^{(2)}}{\beta_0} \frac{y}{1-y} + \frac{A_g^{(2)} \beta_1}{\beta_0^3} \frac{y(3y-2) - 2(1-2y) \ln(1-y)}{2(1-y)^2} \\ &\quad + \frac{A_g^{(1)}}{\beta_0^4} \left(\frac{\beta_1^2(1-2y) \ln^2(1-y)}{2(1-y)^2} + \ln(1-y) \left(\beta_0 \beta_2 - \beta_1^2 + \frac{\beta_1^2}{1-y}\right) \right. \\ &\quad \left. + \frac{y(\beta_0 \beta_2(2-3y) + \beta_1^2 y)}{2(1-y)^2}\right) + \frac{B_g^{(1)} \beta_1}{\beta_0^2} \frac{y + \ln(1-y)}{1-y} - \frac{A_g^{(1)}}{2} \frac{y^2}{(1-y)^2} \ln^2\left(\frac{Q^2}{\mu_R^2}\right) \\ &\quad + \left(B_g^{(1)} \frac{y}{1-y} + \frac{A_g^{(2)}}{\beta_0} \frac{y^2}{(1-y)^2} + A_g^{(1)} \frac{\beta_1}{\beta_0^2} \left(\frac{y}{1-y} + \frac{(1-2y) \ln(1-y)}{(1-y)^2}\right)\right) \ln\left(\frac{Q^2}{\mu_R^2}\right). \end{aligned} \quad (2.19)$$

Now, the actual integral we require is

$$F_g(\alpha_S, \lambda) \equiv 2 \int_0^Q \frac{dq}{q} \left[2A_g(\alpha_S(q)) \ln \frac{Q}{q} + B_g(\alpha_S(q)) \right] (1 - e^{iq\tau}) \quad (2.20)$$

and so we must introduce $(1 - e^{iq\tau})$ in the integrand. The analogue of Eq. (2.18) is

$$\int_0^Q \frac{dq}{q} f\left(\ln \frac{Q}{q}\right) (1 - e^{iq\tau}) = f\left(\frac{d}{du}\right) \mathcal{J}(Q\tau; -u) \Big|_{u=0} \quad (2.21)$$

where the generating function

$$\begin{aligned} \mathcal{J}(Q\tau; u) &= \int_0^Q \frac{dq}{q} \left(\frac{q}{Q}\right)^u (1 - e^{iq\tau}) \\ &= \frac{1}{u} - (-iQ\tau)^{-u} \gamma(u, -iQ\tau), \end{aligned} \quad (2.22)$$

$\gamma(u, z)$ being the incomplete gamma function,

$$\gamma(u, z) = \Gamma(u) - z^{u-1} e^{-z} \sum_{k=0}^{\infty} \frac{\Gamma(u)}{\Gamma(u-k)} z^{-k}. \quad (2.23)$$

The series represents power corrections, which we do not wish to include in the resummation, so we write instead

$$\begin{aligned}\mathcal{J}(Q\tau; -u) &= \frac{1}{u} [(-iQ\tau)^u \Gamma(1-u) - 1] \\ &= \frac{1}{u} \left[\exp \left(\lambda u + \sum_{k=2} \frac{\zeta_k}{k} u^k \right) - 1 \right] \equiv \frac{1}{u} [e^{\lambda u} Z(u) - 1]\end{aligned}\quad (2.24)$$

where now

$$\lambda = \ln \left(\frac{Q\tau}{i\tau_0} \right), \quad (2.25)$$

i.e. we have chosen $Q_0 = ie^{-\gamma_E}/\tau = i\tau_0/\tau$ in (2.17), and

$$Z(u) \equiv \exp \left(\sum_{k=2} \frac{\zeta_k}{k} u^k \right) = \tau_0^u \Gamma(1-u). \quad (2.26)$$

Now

$$\frac{1}{u} [e^{\lambda u} Z(u) - 1] = \frac{Z(u)}{u} [e^{\lambda u} - 1] + \frac{1}{u} [Z(u) - 1] \quad (2.27)$$

and the second term involves no logarithms, so again we drop it from the resummation. We show in Appendix A that the first term implies that

$$F_g(\alpha_S, \lambda) \equiv 2 \int_0^Q \frac{dq}{q} \left[2A_g(\alpha_S(q)) \ln \frac{Q}{q} + B_g(\alpha_S(q)) \right] (1 - e^{iq\tau}) = -Z \left(\frac{d}{d\lambda} \right) G_g(\alpha_S, 2\lambda), \quad (2.28)$$

where G_g was defined in Eq. (2.14). Now

$$Z \left(\frac{d}{d\lambda} \right) = 1 + \frac{\zeta_2}{2} \frac{d^2}{d\lambda^2} + \frac{\zeta_3}{3} \frac{d^3}{d\lambda^3} + \dots \quad (2.29)$$

where $\zeta_2 = \pi^2/6$, so

$$F_g(\alpha_S, \lambda) = -2\lambda g_1(y) - g_2(y) - a_R \tilde{g}_3(y) + \dots \quad (2.30)$$

where

$$\begin{aligned}\tilde{g}_3(y) &= g_3(y) + \frac{\pi^2}{12a_R} \frac{d^2}{d\lambda^2} [2\lambda g_1(y)] \\ &= g_3(y) - \frac{\pi^2}{3} \frac{A_g^{(1)}}{(1-y)^2}.\end{aligned}\quad (2.31)$$

The other terms from (2.29) contribute logarithms only at the level of g_4 and beyond, so we do not consider them.

Following Ref. [11], we can now enforce the ‘unitarity’ condition, $F_g \rightarrow 0$ as $\tau \rightarrow 0$, by a shift of argument of the logarithm:

$$\lambda \rightarrow \tilde{\lambda} = \ln \left(1 + \frac{Q\tau}{i\tau_0} \right) = \frac{1}{2} \ln \left(1 + \frac{Q^2\tau^2}{\tau_0^2} \right) - i \arctan \left(\frac{Q\tau}{\tau_0} \right), \quad (2.32)$$

so that now $y = 2\beta_0\alpha_S(\mu_R^2)\tilde{\lambda}/\pi$. We must apply a corresponding shift in the factorization scale of the parton distributions and coefficient functions (given explicitly below in Eqs. (3.6)). They are now evaluated at a scale of

$$\tilde{\mu}_F = \frac{Q}{\sqrt{1 + Q^2\tau^2/\tau_0^2}} \quad (2.33)$$

instead of $\mu_F = \tau_0/\tau$, and one must also replace $\alpha_S(\mu_F)/2$ in the coefficient of $R_g^{(I)}$ by

$$\frac{\alpha_S(\tilde{\mu}_F)}{\pi} \arctan\left(\frac{Q\tau}{\tau_0}\right). \quad (2.34)$$

We show in Appendix B that the vanishing of the transverse-energy distribution for $E_T < 0$ implies a dispersion relation between the real and imaginary parts of its Fourier transform. This allows (2.11) to be written in the simpler equivalent form

$$\begin{aligned} \left[\frac{d\sigma_H}{dQ^2 dE_T}\right]_{\text{res.}} &= \frac{2}{\pi s} \int_0^\infty d\tau e^{-F_g^{(R)}(Q,\tau)} \cos(\tau E_T) \left[R_g^{(R)}(s; Q, \tau) \cos\{F_g^{(I)}(Q, \tau)\} \right. \\ &\quad \left. - R_g^{(I)}(s; Q, \tau) \sin\{F_g^{(I)}(Q, \tau)\} \right] \sigma_{gg}^H(Q, \alpha_S(Q)) \end{aligned} \quad (2.35)$$

and implies that

$$\int_0^\infty dE_T \left[\frac{d\sigma_H}{dQ^2 dE_T}\right]_{\text{res.}} = \frac{1}{s} R_g^{(R)}(s; Q, 0) \sigma_{gg}^H(Q, \alpha_S(Q)), \quad (2.36)$$

where, on account of (2.33), the parton distributions in $R_g^{(R)}(s; Q, 0)$ are evaluated at scale Q .

3. Matching to fixed order

We now match the resummed expression derived above to the NLO perturbative expansion of the transverse energy distribution, taking care to avoid double counting of the terms already contained in the resummation.

3.1 Expansion of the resummed prediction

Performing the expansion of Eq. (2.30) in powers of $a_R \equiv \alpha_S(\mu_R^2)/\pi$, we find

$$\begin{aligned} -2\lambda g_1 &= 2A_g^{(1)}\lambda^2 a_R + \frac{8}{3}\beta_0 A_g^{(1)}\lambda^3 a_R^2 + \mathcal{O}(a_R^3) \\ -g_2 &= 2B_g^{(1)}\lambda a_R + 2 \left[A_g^{(2)} + \beta_0 B_g^{(1)} - \beta_0 A_g^{(1)} \ln\left(\frac{Q^2}{\mu_R^2}\right) \right] \lambda^2 a_R^2 + \mathcal{O}(a_R^3) \\ -a_R \tilde{g}_3 &= \frac{\pi^2}{3} A_g^{(1)} a_R + 2 \left[B_g^{(2)} + \frac{2}{3}\pi^2 \beta_0 A_g^{(1)} - \beta_0 B_g^{(1)} \ln\left(\frac{Q^2}{\mu_R^2}\right) \right] \lambda a_R^2 + \mathcal{O}(a_R^3), \end{aligned} \quad (3.1)$$

so that to NLO

$$F_g(\alpha_S, \lambda) = a_R F_1 + a_R^2 F_2 \quad (3.2)$$

where, following the shift $\lambda \rightarrow \tilde{\lambda}$ according to Eq. (2.32)

$$\begin{aligned}
F_1 &= 2A_g^{(1)} \left(\tilde{\lambda}^2 + \frac{\pi^2}{6} \right) + 2B_g^{(1)} \tilde{\lambda} \\
F_2 &= \frac{8}{3} \beta_0 A_g^{(1)} \tilde{\lambda}^3 + 2 \left[A_g^{(2)} + \beta_0 B_g^{(1)} - \beta_0 A_g^{(1)} \ln \left(\frac{Q^2}{\mu_R^2} \right) \right] \tilde{\lambda}^2 \\
&\quad + 2 \left[B_g^{(2)} + \frac{2}{3} \pi^2 \beta_0 A_g^{(1)} - \beta_0 B_g^{(1)} \ln \left(\frac{Q^2}{\mu_R^2} \right) \right] \tilde{\lambda}.
\end{aligned} \tag{3.3}$$

Similarly, evaluating all PDFs at scale $\mu = Q$, we can write to NLO

$$R_g(\tau) = R_0 + a_R \left(R_1 + \tilde{\lambda} R'_1 \right) + a_R^2 \left(R_2 + \tilde{\lambda} R'_2 + \tilde{\lambda}^2 R''_2 \right) \tag{3.4}$$

so that

$$\begin{aligned}
S_g R_g &= R_0 + a_R R_1 + a_R^2 R_2 + a_R \left(\tilde{\lambda} R'_1 - F_1 R_0 \right) \\
&\quad + a_R^2 \left[\tilde{\lambda} R'_2 + \tilde{\lambda}^2 R''_2 - \left(F_2 - \frac{1}{2} F_1^2 \right) R_0 - F_1 \left(R_1 + \tilde{\lambda} R'_1 \right) \right]
\end{aligned} \tag{3.5}$$

where

$$\begin{aligned}
R_0 &= \int_{\xi}^1 \frac{dx_1}{x_1} f_g(x_1) f_g \left(\frac{\xi}{x_1} \right) \\
R_1 &= \int_{\xi}^1 \frac{dx_1}{x_1} \left\{ 2c_g^{(1)} f_g(x_1) f_g \left(\frac{\xi}{x_1} \right) + C_F \int_{\xi/x_1}^1 dz f_s(x_1) f_g \left(\frac{\xi}{zx_1} \right) \right\} \\
R'_1 &= - \int_{\xi}^1 \frac{dx_1}{x_1} \left\{ 2f_g(x_1) f_g \left(\frac{\xi}{x_1} \right) \left[2C_A \ln \left(1 - \frac{\xi}{x_1} \right) + \frac{1}{6} (11C_A - 2n_f) \right] \right. \\
&\quad + \int_{\xi/x_1}^1 \frac{dz}{z} \left[4C_A f_g(x_1) \left\{ f_g \left(\frac{\xi}{zx_1} \right) \left[\frac{z}{1-z} + \frac{1-z}{z} + z(1-z) \right] - f_g \left(\frac{\xi}{x_1} \right) \frac{z}{1-z} \right\} \right. \\
&\quad \left. \left. + 2C_F f_s(x_1) f_g \left(\frac{\xi}{zx_1} \right) \frac{1 + (1-z)^2}{z} \right] \right\}.
\end{aligned} \tag{3.6}$$

Performing the Fourier transformation (2.1), we find terms involving the integrals

$$\mathcal{I}_p(E_T, Q) = \frac{1}{2\pi} \int_{-\infty}^{+\infty} d\tau e^{-i\tau E_T} \ln^p \left(1 + \frac{Q\tau}{i\tau_0} \right) \tag{3.7}$$

with $p = 1, 2, 3, 4$, which may be evaluated from

$$\mathcal{I}_p(E_T, Q) = \frac{d^p}{du^p} \mathcal{I}(E_T, Q; u) \Big|_{u=0} \tag{3.8}$$

with generating function

$$\mathcal{I}(E_T, Q; u) = \frac{1}{2\pi} \int_{-\infty}^{+\infty} d\tau e^{-i\tau E_T} \left(1 + \frac{Q\tau}{i\tau_0} \right)^u. \tag{3.9}$$

Writing

$$1 + \frac{Q\tau}{i\tau_0} = \frac{zQ}{\tau_0 E_T} \quad (3.10)$$

we have

$$\mathcal{I}(E_T, Q; u) = -\frac{i}{2\pi E_T} \left(\frac{Q}{E_T \tau_0} \right)^u \int_{-i\infty}^{+i\infty} dz z^u e^{z - \tau_0 E_T / Q}. \quad (3.11)$$

We can safely deform the integration contour around the branch cut along the negative real axis to obtain

$$\begin{aligned} \mathcal{I}(E_T, Q; u) &= -\frac{u}{E_T} \left(\frac{Q}{E_T} \right)^u \frac{\exp(u\gamma_E - \tau_0 E_T / Q)}{\Gamma(1-u)} \\ &= -\frac{u}{E_T} \left(\frac{Q}{E_T} \right)^u \exp\left(-\frac{\tau_0 E_T}{Q} - \sum_{k=2}^{\infty} \frac{\zeta_k}{k} u^k \right). \end{aligned} \quad (3.12)$$

This gives

$$\begin{aligned} \mathcal{I}_1(E_T, Q) &= -\frac{1}{E_T} e^{-\tau_0 E_T / Q} \\ \mathcal{I}_2(E_T, Q) &= -\frac{2}{E_T} \ln\left(\frac{Q}{E_T} \right) e^{-\tau_0 E_T / Q} \\ \mathcal{I}_3(E_T, Q) &= -\frac{3}{E_T} \left[\ln^2\left(\frac{Q}{E_T} \right) - \frac{\pi^2}{6} \right] e^{-\tau_0 E_T / Q} \\ \mathcal{I}_4(E_T, Q) &= -\frac{4}{E_T} \left[\ln^3\left(\frac{Q}{E_T} \right) - \frac{\pi^2}{2} \ln\left(\frac{Q}{E_T} \right) - 2\zeta_3 \right] e^{-\tau_0 E_T / Q}. \end{aligned} \quad (3.13)$$

Therefore the NLO expansion of the resummed expression is

$$\begin{aligned} \left[\frac{E_T d\sigma_H}{\sigma_0^H dE_T} \right]_{\text{resum, NLO}} &= \left[a_R(G_0 R_0 + G'_1 R'_1) + a_R^2(H_0 R_0 + H_1 R_1 \right. \\ &\quad \left. + H'_1 R'_1 + H'_2 R'_2 + H''_2 R''_2) \right] e^{-\tau_0 E_T / Q} \end{aligned} \quad (3.14)$$

where, writing $L = \ln(Q/E_T)$,

$$\begin{aligned} G_0 &= H_1 = 4A_g^{(1)}L + 2B_g^{(1)}, \quad G'_1 = -1, \\ H_0 &= 4L \left[A_g^{(2)} + \beta_0 B_g^{(1)} - \beta_0 A_g^{(1)} \ln\left(\frac{Q^2}{\mu_R^2} \right) \right] + 8\beta_0 A_g^{(1)} \left(L^2 - \frac{\pi^2}{6} \right) \\ &\quad + 2 \left[B_g^{(2)} + \frac{2}{3}\pi^2 \beta_0 A_g^{(1)} - \beta_0 B_g^{(1)} \ln\left(\frac{Q^2}{\mu_R^2} \right) \right] - 8(A_g^{(1)})^2 \left(L^3 - \frac{\pi^2}{3}L - 2\zeta_3 \right) \\ &\quad - 12A_g^{(1)}B_g^{(1)} \left(L^2 - \frac{\pi^2}{9} \right) - 4(B_g^{(1)})^2 L, \\ H'_1 &= 6A_g^{(1)} \left(L^2 - \frac{\pi^2}{9} \right) + 4B_g^{(1)}L, \quad H'_2 = -1, \quad H''_2 = -2L. \end{aligned} \quad (3.15)$$

We evaluate the coefficients R_0, R_1, R'_1 explicitly from Eqs. (3.6), and then obtain the higher-order coefficients R'_2, R''_2 from a fit to the Higgs transverse-momentum distribution,

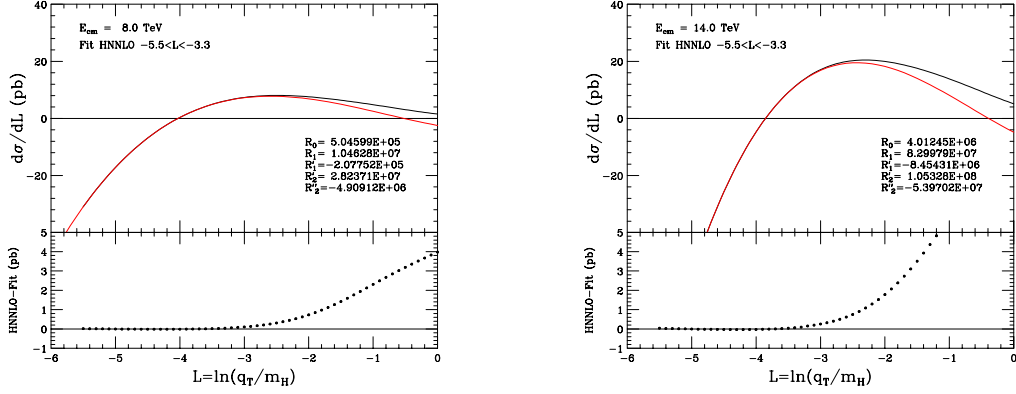


Figure 1: Upper panels: fits to the logarithmic terms of the transverse-momentum (q_T) distribution in Higgs boson production at the LHC at 8 and 14 TeV. Black: NLO data from HNNLO. Red: fit to data at $-5.5 < L < -3.3$. Lower panels: difference between the NLO data and the fits.

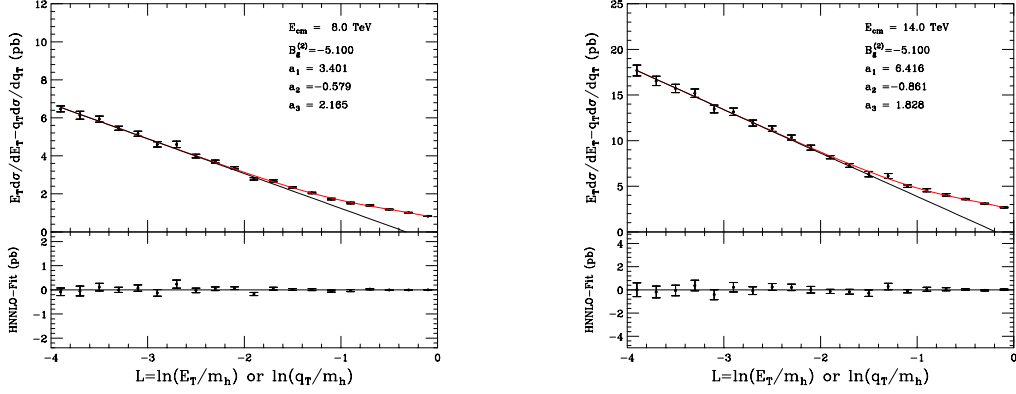


Figure 2: Upper panels: fits to the difference between the transverse-energy (E_T) and transverse-momentum (q_T) distribution in Higgs boson production at the LHC at 8 and 14 TeV. Points: NLO data from HNNLO. Red: fit to data. Black: logarithmic terms only. Lower panels: difference between the NLO data and the fits.

as explained in Appendix C. These coefficients depend only on the parton distribution functions and the NLO coefficient functions $C_{ga}^{(1)}$, which are the same for the E_T and q_T spectra. Using the MSTW 2008 NLO parton distributions [27], we find the values indicated in Fig. 1, where the resulting fits are also shown.

3.2 Matching to NLO

The NLO prediction for the transverse-energy distribution is conveniently obtained from the known NLO transverse-momentum distribution by adding the difference between the two distributions, obtained from Higgs plus two-jet production at leading order. Given

the value of $B_g^{(2)}$ for the transverse-energy distribution, the NLO prediction (C.8) for the difference at small E_T is independent of the fitted parameters R'_2, R''_2 . From HNNLO [28, 29] data on this quantity at 8 and 14 TeV, shown in Fig. 2, we find consistent best-fit $B_g^{(2)}$ values of -4.5 ± 2.1 and -6.0 ± 2.6 , respectively, with weighted average $B_g^{(2)} = -5.1 \pm 1.6$. This is significantly different from the value of $\bar{B}_g^{(2)} = 26.8$ given by Eqs. (2.9) for the transverse-momentum distribution. We will use $B_g^{(2)} = -5.1$ from now on.

Away from the small- E_T region, the NLO data are then well described by a parametrization of the form

$$\left[\frac{d\sigma_H}{dE_T} - \frac{d\sigma_H}{dq_T} \Big|_{q_T=E_T} \right]_{\text{NLO}} = \text{Logarithmic terms} + \frac{a_1 E_T}{m_H(m_H + a_2 E_T) + a_3 E_T^2}, \quad (3.16)$$

as shown by the red curves in Fig. 2, with the parameter values shown.

To match the resummed and NLO E_T distributions, we have to subtract the NLO logarithmic terms (3.14), which are already included in the resummation, and replace them by the full NLO result:

$$\frac{d\sigma_H}{dE_T} = \left[\frac{d\sigma_H}{dE_T} \right]_{\text{resum}} - \left[\frac{d\sigma_H}{dE_T} \right]_{\text{resum,NLO}} + \left[\frac{d\sigma_H}{dE_T} \right]_{\text{NLO}}. \quad (3.17)$$

3.3 Results

In the following we present numerical results for our resummed calculation of the E_T distribution at the LHC. Our resummed results are obtained by using Eq. (3.17): the resummed component is evaluated by including the coefficients $C_{ga}^{(1)}$ in Eq. (2.9), and the functions g_1, g_2 and g_3 of Eqs. (2.19). The required coefficients $A_g^{(1)}, A_g^{(2)}$ and $B_g^{(1)}$ are given in Eq. (2.9). For the coefficient $B_g^{(2)}$ we use the numerical value extracted in Sec. 3.2. The unknown coefficient $A_g^{(3)}$ is neglected. We will comment later on the numerical impact of the missing $A_g^{(3)}$ and $C_{ga}^{(2)}$ coefficients.

The resulting resummed and matched E_T distributions at the LHC at 8 and 14 TeV are shown in Fig. 3. For all these predictions we use the best-fit value $B_g^{(2)} = -5.1$ found from the NLO data. The distribution peaks at around $E_T = 35$ GeV at both centre-of-mass energies, considerably above the peak in the Higgs transverse-momentum distribution, around $q_T = 12$ GeV [11]. Thus in the peak region of E_T the resummed logarithms are not so dominant as in the corresponding region of q_T . On the other hand, the fixed-order NLO prediction is rising rapidly and unphysically towards smaller values of E_T .³

The purely resummed distribution becomes slightly negative at small and large E_T , which is also unphysical. The effect of matching is to raise the distribution to positive values, close to the fixed-order prediction at high E_T . The matched prediction is still somewhat unstable at small E_T , owing to the delicate cancellation of diverging logarithmic terms. The behaviour at large E_T has been significantly improved compared to the results of Ref. [3] where matching was only performed to leading order. The renormalization scale dependence is comparable to that of the NLO result above and around the peak of the

³At very small E_T it turns over and tends to $-\infty$, as seen in Fig. 1.

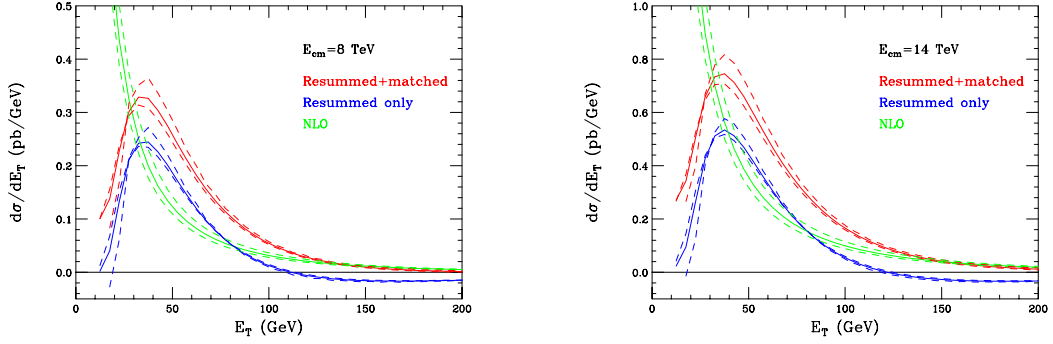


Figure 3: Transverse-energy distribution in Higgs boson production at the LHC at 8 and 14 TeV. Blue: resummed only. Red: resummed and matched to NLO. Green: NLO only. The solid curves correspond to renormalization scale m_H , the dashed to $2m_H$ and $m_H/2$.

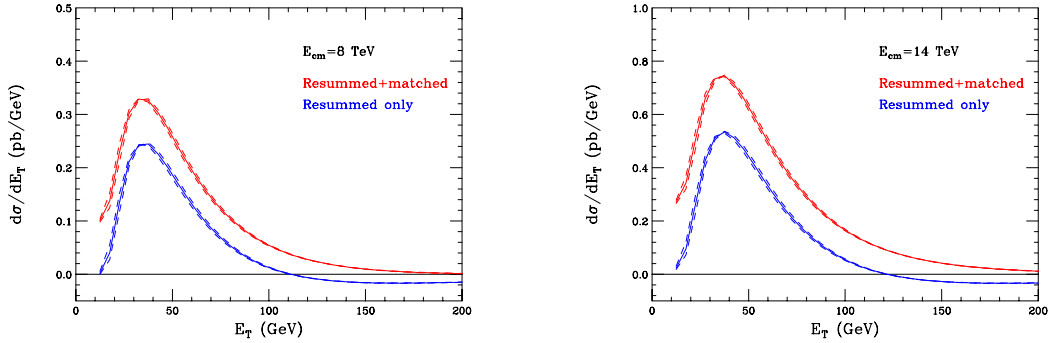


Figure 4: Transverse-energy distribution in Higgs boson production at the LHC at 8 and 14 TeV. Blue: resummed only. Red: resummed and matched to NLO. The solid curves correspond to $A_g^{(3)} = 0$, the dashed to $A_g^{(3)} = \pm 30$.

distribution, but changes sign at lower E_T , with smaller scales giving a lower cross section there and a peak that is higher and shifted to slightly larger E_T .

As a result of the unitarity condition (2.36) and the matching to fixed order, the cross section integrated over all E_T should be equal to the NNLO inclusive Higgs cross section, within the uncertainties due to the unknown coefficients. Integrating up to $E_T = 760$ GeV, we obtain resummed matched cross sections of 18.4 pb and 47.8 pb at 8 and 14 TeV, respectively, which compare well with the NNLO inclusive values of 18.22 pb and 47.28 pb, computed with the same NLO PDFs and two-loop α_S .

As mentioned above, the leading terms that are neglected in our analysis correspond to the coefficient $A_g^{(3)}$ in Eq. (2.6) and the coefficient functions $C_{ga}^{(2)}(z)$ in (2.8). In Fig. 4

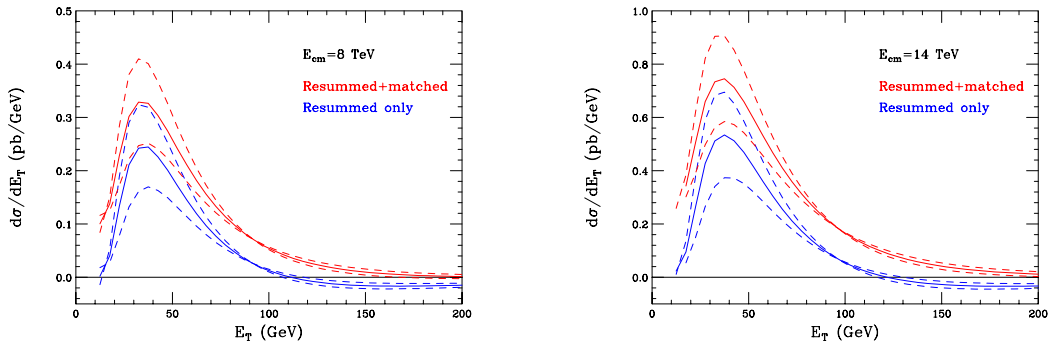


Figure 5: Transverse-energy distribution in Higgs boson production at the LHC at 8 and 14 TeV. Blue: resummed only. Red: resummed and matched to NLO. The solid curves correspond to $C_g^{(2)} = 0$, the dashed to $C_g^{(2)} = \pm 115.5$ (see text).

we show the sensitivity of the prediction to $A_g^{(3)}$, assuming a value similar in magnitude to that used for the q_T distribution in Ref. [11]. As was found there, the effect of including this coefficient is small.

The NNLO coefficient functions $C_{ga}^{(2)}(z)$ were computed for the Higgs transverse-momentum distribution in Ref. [30], where it was found that their dominant effect could be approximated as

$$\overline{C}_{ga}^{(2)}(z) \approx \overline{C}_g^{(2)} \delta_{ag} \delta(1-z) \quad (3.18)$$

where $\overline{C}_g^{(2)} = 115.5$. In Fig. 5 we show the effects of assuming the same form and magnitude for the corresponding coefficient in E_T resummation. We see that the effect is larger than that of $A_g^{(3)}$ and of renormalization scale variation. Thus in this case uncertainties in the higher-order coefficient functions provide a more conservative error estimate than the usual range of scale variation.

4. Monte Carlo studies

Up to this point we have only considered the perturbative contributions to the E_T distribution that arise due to initial state radiation (ISR). However, there are important contributions to the E_T originating from non-perturbative effects such as hadronization and the underlying event (UE). Moreover, the distributions can be altered further because of cuts imposed either due to the detector geometry, or to accommodate the experimental analyses.

All of the aforementioned effects on the E_T distribution are challenging to predict analytically. Therefore, we make the assumption that the kinematics of the process, apart from the UE, is governed predominantly by the shape of the E_T distribution. Under this assumption, one can reweight the parton-level E_T of a Monte Carlo event generator (i.e.

with the UE and hadronization turned off), to the one calculated analytically, and use the phenomenological models of the Monte Carlo to estimate the features of the effects.

Taking into account the non-perturbative and detector geometry effects, one may construct a quantity that is, at least in principle, close to what can be measured experimentally:

$$E_T = \sum_{\substack{|\eta_i| < \eta^c \\ |\mathbf{p}_{Ti}| > p_T^c}} |\mathbf{p}_{Ti}|, \quad (4.1)$$

where the sum is taken over the hadrons in the event, with p_T^c and η^c their minimum transverse momentum and maximum pseudorapidity respectively. The effect of these cuts will be investigated below.⁴

4.1 E_T at parton level

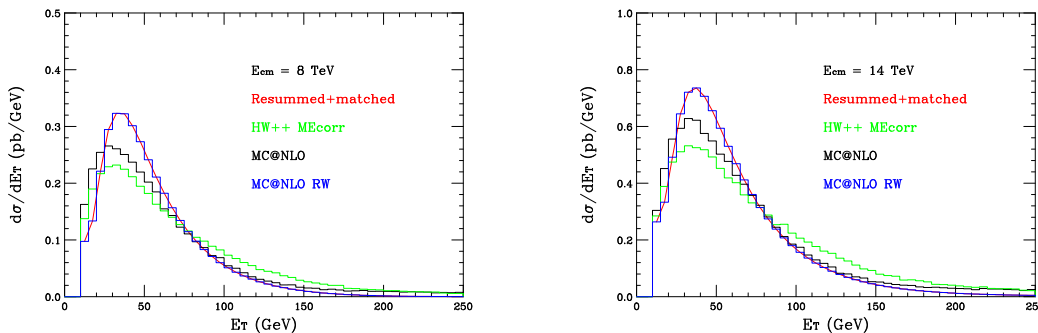


Figure 6: Parton-level transverse-energy distribution in Higgs boson production at the LHC at 8 and 14 TeV. Red: resummed and matched to NLO. Green: `Herwig++` with Matrix Element correction, no reweighting. Black: `aMC@NLO+Herwig++` before reweighting. Blue: `aMC@NLO+Herwig++` after reweighting.

Here we employ the `Herwig++` general-purpose event generator (version 2.6.3) [31, 32] in conjunction with events generated using `aMC@NLO` [33, 34]. For purposes of comparison with alternative descriptions of the parton shower, hadronization and the underlying event, we additionally verify the `Herwig++` results using the `Pythia8` event generator [35, 36]. The distributions found using `Pythia8` are very similar to those obtained with `Herwig++` and thus we defer them to Appendix D.

Use of `aMC@NLO` ensures correct treatment of the NLO inclusive cross section matched to parton showers without double counting. We assign a new weight to each event so as to reproduce the analytic resummed and matched distributions shown in Fig. 3. For completeness, we show in Fig. 6 the resulting E_T distributions before and after the reweighting, at parton level, demonstrating that this procedure reproduces the analytic result. Higgs

⁴The E_T distribution may also be constructed using jets. It is not feasible, however, to reconstruct the parton- or hadron-level distributions from the jet-level distributions.

boson production using the internal `Herwig++` implementation, which includes Matrix Element (ME) corrections⁵, is also shown on the figure. The ME-corrected E_T distribution has a lower peak and consequently falls off more slowly at higher E_T than the MC@NLO case. In Fig. 7 we show the Higgs boson transverse-momentum distribution, q_T , before and after applying the reweighting procedure, compared to the equivalent distribution obtained by the HQT program [11, 37]. Evidently, the MC@NLO distribution agrees already quite well with the HQT prediction before reweighting. The reweighting procedure improves agreement in the peak region but makes the distribution fall off faster at high q_T , which is consistent with the change in shape observed in Fig. 6. Figure 8 shows the rapidity distribution of the Higgs boson, y_H , before and after the reweighting, clearly showing that the effect on this distribution is negligible, thus verifying that the reweighting does not alter physics in the forward direction.

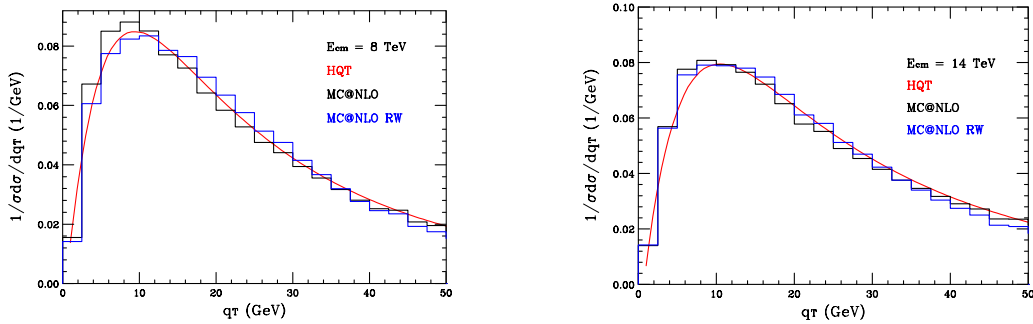


Figure 7: Higgs boson transverse-momentum distribution at the LHC at 8 and 14 TeV. Red: HQT calculation. Black: `aMC@NLO+Herwig++` before reweighting. Blue: `aMC@NLO+Herwig++` after reweighting.

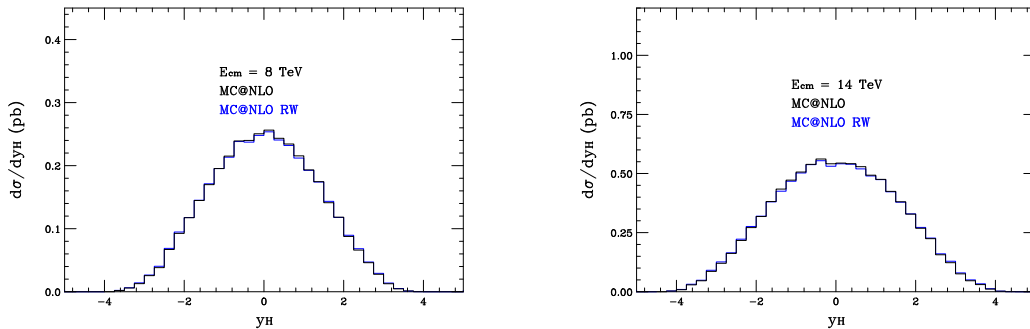


Figure 8: Higgs boson rapidity distribution at the LHC at 8 and 14 TeV. Black: `aMC@NLO+Herwig++` before reweighting. Blue: `aMC@NLO+Herwig++` after reweighting.

⁵The ME corrections include the higher-order tree-level contributions $gg \rightarrow hg$, $q\bar{q} \rightarrow hq$, $g\bar{q} \rightarrow h\bar{q}$ and $q\bar{q} \rightarrow hg$.

4.2 E_T at hadron level

The effects of hadronization can be studied by enabling the cluster hadronization model in the `Herwig++` event generator in conjunction with the reweighting. The default parameters of the hadronization model available in `Herwig++` version 2.6.3 were used. The effect is to shift the peak of the distribution to higher E_T , by about 15 GeV at both 8 TeV and 14 TeV, as shown in Fig. 9. The effect of hadronization on the E_T distribution can be compensated almost completely in this range of values by imposing a pseudorapidity cut on the hadrons contributing to the E_T , allowing only hadrons within $|\eta| < 5$ to enter. The resulting distributions after this cut are also shown in Fig. 9. We note that including the restriction on hadrons of $|\eta| < 5$ approximately corresponds to the experimental detector coverage of the ATLAS and CMS detectors.

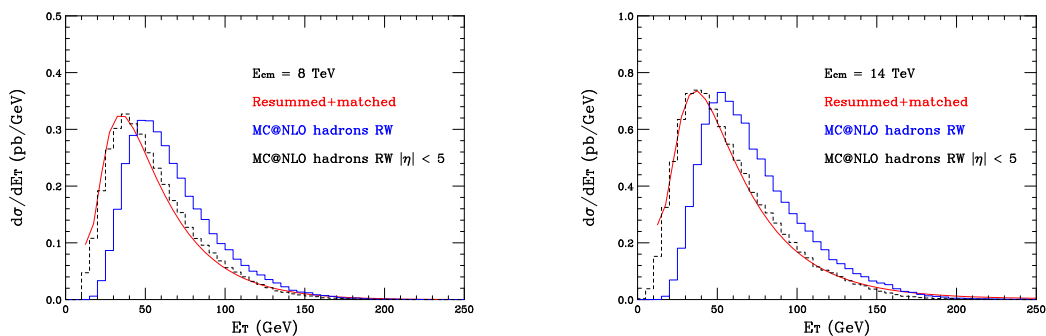


Figure 9: Hadron-level transverse-energy distribution in Higgs boson production at the LHC at 8 and 14 TeV. Red: resummed and matched to NLO. Blue: `aMC@NLO+Herwig++` after reweighting. Black dashes: `aMC@NLO+Herwig++` after reweighting, particles restricted to lie within pseudorapidity $|\eta| < 5$.

4.3 Inclusion of the underlying event

The underlying event (UE) is thought to arise due to secondary multiple interactions between the colliding hadrons. The model present in `Herwig++` is based on the eikonal model formulated in Refs. [38–40]. The underlying event activity is treated as additional semi-hard and soft partonic scatters. In this version, a model of colour reconnection has been added to `HERWIG++`, based on the idea of colour preconfinement, which provides an improved description of underlying event data at the LHC [41].

The effect of the UE on the E_T distributions is severe, making them much broader and moving the peak to much higher values of E_T . This was investigated in Ref. [3] at parton level, where it was shown that in the `Herwig++` model the E_T distribution for the partons originating from the UE is approximately independent of the nature of the hard process. This distribution was fitted with a Fermi distribution and was shown to reproduce the total distribution after convolution with the perturbative result.⁶

⁶This approach, however, predicts distributions only at parton-level.

We present results using the default parameters present in `Herwig++` version 2.6.3 for the underlying event model. We note that these were tuned to a variety of experimental data using the MRST LO** PDF set [42] instead of the MSTW2008 NLO set [27] used here for the hard process generated using `aMC@NLO`.⁷ In Fig. 10 we show the E_T distribution including the UE, with hadrons of a maximum pseudorapidity $\eta^c = 5$, compared against the analytical result, which we have shown matches well the hadron-level $\eta^c = 5$ distribution without UE (Fig. 9). In practice, particles cannot be detected at transverse momenta down to zero, and therefore we show the effect of applying transverse-momentum cuts on the hadrons: $p_T^c = 1.0, 1.5, 2.0$ GeV. When $p_T^c = 1.5$ GeV the peak in E_T is moved back to approximately the value of the parton-level prediction, but the distribution itself is still somewhat broader.

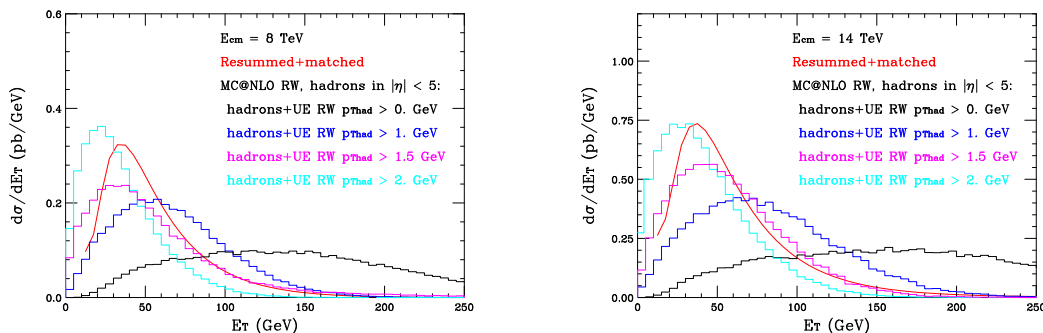


Figure 10: Hadron-level transverse-energy distribution in Higgs boson production at the LHC at 8 and 14 TeV, including the effect of the underlying event. Red: resummed and matched to NLO, for comparison. Reweighted `aMC@NLO+Herwig++` events with hadron maximum pseudorapidity $\eta^c = 5$: Black: $p_T^c = 0$ GeV, Blue: $p_T^c = 1.0$ GeV, Magenta: $p_T^c = 1.5$ GeV, Cyan: $p_T^c = 2.0$ GeV.

We have also investigated the impact of the underlying event using different PDFs and different, reasonable, model parameters. We found that, with reasonably-tuned values for the underlying event model parameters, the change of PDF sets does not induce any significant changes to the distributions.

To conclude, one can reproduce the E_T distribution with the effect of the UE and detector geometry effects by reweighting the parton-level Monte Carlo events to match the analytical prediction of the E_T due to ISR and subsequently enabling the hadronization and underlying event models of the generator. The description of the underlying event is robust against changes of tune parameters as well as PDF sets. However, in the presence of the underlying event the E_T distribution is highly sensitive to the minimum hadron transverse momentum, p_T^c .

⁷MRST LO**, the default PDF set for LO processes in `Herwig++`, is called ‘MRSTMCal’, with set number 20651 in the LHAPDF database [43].

5. Conclusions

We have presented the first detailed predictions of the transverse-energy distribution in Higgs boson production at the LHC ($\sqrt{s} = 8$ and 14 TeV) for $m_H = 126$ GeV. Our calculation includes the resummation of the large logarithmic terms at small E_T up to (almost) NNLL accuracy, matched to the fixed-order NLO result in a way that limits the impact of the resummation in the intermediate and large- E_T regions.

Our main result for the resummation is Eq. (2.35), with component expressions (2.13), (2.19) and (2.30). For the matching we have Eq. (3.17) with (3.6), (3.14) and (3.15). The resulting predictions are shown in Fig. 3. The effect of resummation, compared to the pure NLO result, is large over the whole range of E_T . The purely resummed distribution peaks at around 35 GeV and falls to unphysical negative values at small and large E_T . This behaviour is rectified by matching, which also provides the NNLO normalization, without shifting the peak significantly. The uncertainty in the prediction, as assessed by the customary factor-of-two variation of the renormalization scale, is of the order of $\pm 10\%$. However, the sensitivity to unknown terms beyond NLO, in particular the NNLO coefficient function $C_g^{(2)}$, is considerable, suggesting a larger uncertainty. The possible impacts of $C_g^{(2)}$ and the neglected NNLL coefficient $A_g^{(3)}$ were illustrated in Figs. 5 and 4 respectively.

The resummed and matched predictions refer only to the perturbative hard-scattering component of Higgs production. In real events there are the non-perturbative effects of hadronization and the underlying event. We made a Monte Carlo study of these effects using `aMC@NLO` interfaced to `Herwig++` or `Pythia8`, which provide a state-of-the-art simulation of complete LHC final states. The simulated events were reweighted at the parton level to reproduce the analytically resummed and matched E_T distribution. The effect of hadronization was to shift the peak of the distribution upwards, to around 50 GeV, if all produced hadrons were included. However, this effect was practically eliminated by a pseudorapidity cut $|\eta_{\text{had}}| < 5$. The effect of the underlying event was much greater, even in the presence of the pseudorapidity cut, the E_T distribution becoming much broader, as was found in Ref. [3]. This effect is due to soft hadrons in the underlying event; a cut on hadron transverse momenta $p_{T\text{had}} > 1.5$ GeV restored the E_T peak to around 30-40 GeV, although with a distribution still somewhat broader than the parton-level prediction.

Measurements of differential distributions of the Higgs boson at the LHC are starting to appear [44]. We look forward to measurement of the transverse-energy distribution and to comparisons with our theoretical predictions.

Acknowledgements

AP thanks Paolo Torrielli and Stefan Prestel for help in using the `aMC@NLO` and `Pythia8` packages respectively and acknowledges support by the Swiss National Science Foundation under contracts 200020-138206 and 200020-141360/1. AP and BW also acknowledge MC-netITN FP7 Marie Curie Initial Training Network PITN-GA-2012-315877. JMS is funded by a Royal Society University Research Fellowship. BRW acknowledges the partial support of a Leverhulme Trust Emeritus Fellowship and thanks the Pauli Center for Theoretical

Studies, Zurich, and the Kavli IMPU, University of Tokyo, for hospitality and support during parts of this work. The Kavli IPMU is supported by World Premier International Research Center Initiative (WPI Initiative), MEXT, Japan.

A. Proof of an identity

To prove Eq. (2.28), we will show in general that

$$f\left(\frac{d}{du}\right)\frac{Z(u)}{u}\left[e^{\lambda u}-1\right]\Big|_{u=0}=Z\left(\frac{d}{d\lambda}\right)f\left(\frac{d}{du}\right)\frac{1}{u}\left[e^{\lambda u}-1\right]\Big|_{u=0}, \quad (\text{A.1})$$

where f and Z have power series expansions,

$$f(x)=\sum_{\ell}f_{\ell}x^{\ell}, \quad Z(u)=\sum_mZ_mu^m, \quad (\text{A.2})$$

which holds for the functions in Eq. (2.28). Now, beginning with the left-hand side,

$$\frac{1}{u}\left[e^{\lambda u}-1\right]=\sum_{n=0}^{\infty}\frac{\lambda^{n+1}}{(n+1)!}u^n, \quad (\text{A.3})$$

so we can write

$$\begin{aligned} f\left(\frac{d}{du}\right)\frac{Z(u)}{u}\left[e^{\lambda u}-1\right]\Big|_{u=0} &= \sum_{\ell mn}f_{\ell}Z_m\frac{d^{\ell}}{du^{\ell}}\frac{\lambda^{n+1}}{(n+1)!}u^{m+n}\Big|_{u=0} \\ &= \sum_{\ell mn}f_{\ell}Z_m\lambda^{n+1}\frac{(m+n)!}{(n+1)!}\delta_{\ell-m-n} \\ &= \sum_{\ell m}f_{\ell}Z_m\lambda^{\ell-m+1}\frac{\ell!}{(\ell-m+1)!} \\ &= \sum_{\ell m}f_{\ell}Z_m\frac{d^m}{d\lambda^m}\frac{\lambda^{\ell+1}}{(\ell+1)} \\ &= Z\left(\frac{d}{d\lambda}\right)f\left(\frac{d}{du}\right)\frac{1}{u}\left[e^{\lambda u}-1\right]\Big|_{u=0}. \end{aligned} \quad (\text{A.4})$$

B. Dispersion relations

The fact that $d\sigma/dE_T \equiv F(E_T)$ has to vanish for $E_T < 0$ implies that its Fourier transform $G(\tau)$ must satisfy dispersion relations analogous to those in the frequency domain that follow from causality. Note first that if we write

$$F(E_T)=\Theta(E_T)f(E_T), \quad (\text{B.1})$$

where Θ is the Heaviside step-function, then $f(E_T)$ can be chosen to be either an odd or an even function. We choose f even, and then its Fourier transform $g(\tau)$ is purely real. Now the Fourier transform of a product is a convolution, so

$$G(\tau)=\frac{1}{2\pi}\int_{-\infty}^{+\infty}d\tau'h(\tau-\tau')g(\tau') \quad (\text{B.2})$$

where h is the Fourier transform of Θ :

$$h(\tau) = \pi \delta(\tau) + P \frac{i}{\tau}, \quad (\text{B.3})$$

P indicating the principal value. Thus

$$G(\tau) = \frac{1}{2}g(\tau) + \frac{i}{2\pi}P \int_{-\infty}^{+\infty} d\tau' \frac{g(\tau')}{\tau - \tau'}. \quad (\text{B.4})$$

Now writing $G = G_R + iG_I$, recalling that $g(\tau)$ is real and equating real parts we see that

$$g(\tau) = 2G_R(\tau). \quad (\text{B.5})$$

Furthermore G_I is not an independent function: it must satisfy the dispersion relation

$$G_I(\tau) = \frac{1}{\pi}P \int_{-\infty}^{+\infty} d\tau' \frac{G_R(\tau')}{\tau - \tau'}. \quad (\text{B.6})$$

Notice that it follows that $G_R(\tau)$ must be an even function while $G_I(\tau)$ must be odd, i.e. $G(-\tau) = G^*(\tau)$. Altogether, we have

$$G(\tau) = G_R(\tau) + \frac{i}{\pi}P \int_{-\infty}^{+\infty} d\tau' \frac{G_R(\tau')}{\tau - \tau'}. \quad (\text{B.7})$$

Thus

$$F(E_T) = \frac{1}{2\pi} \int_{-\infty}^{+\infty} d\tau e^{-iE_T\tau} \left[G_R(\tau) + \frac{i}{\pi}P \int_{-\infty}^{+\infty} d\tau' \frac{G_R(\tau')}{\tau - \tau'} \right]. \quad (\text{B.8})$$

Assuming that the order of integration can be exchanged, the second term involves

$$I(\tau') \equiv \frac{i}{\pi}P \int_{-\infty}^{+\infty} d\tau \frac{e^{-iE_T\tau}}{\tau - \tau'}. \quad (\text{B.9})$$

The principal value implies the average of integrations along contours above and below the pole at $\tau = \tau'$. The contour can be closed in the lower half-plane, where the exponential vanishes at infinity since $E_T > 0$. Thus

$$I(\tau') = e^{-iE_T\tau'} \quad (\text{B.10})$$

and, relabelling τ' as τ in the second term, we see that the two terms are equal and

$$F(E_T) = \frac{1}{\pi} \int_{-\infty}^{+\infty} d\tau e^{-iE_T\tau} G_R(\tau). \quad (\text{B.11})$$

Thus we can simply replace the full Fourier transform G by twice its real part. Furthermore, since G_R is an even function, it then follows immediately that

$$\int_0^{\infty} F(E_T) dE_T = G_R(0). \quad (\text{B.12})$$

In the notation of Eq. (2.35), we have

$$G_R(\tau) = e^{-F_g^{(R)}(Q,\tau)} \left[R_g^{(R)}(s; Q, \tau) \cos\{F_g^{(I)}(Q, \tau)\} - R_g^{(I)}(s; Q, \tau) \sin\{F_g^{(I)}(Q, \tau)\} \right] \sigma_{gg}^H(Q, \alpha_S(Q)) \quad (\text{B.13})$$

and, by virtue of the shift (2.32), $F_g^{(R)}(Q, 0) = F_g^{(I)}(Q, 0) = 0$, so we obtain Eq. (2.36).

C. Comparison with transverse-momentum resummation

For the Higgs transverse momentum q_T , instead of integrals of the form (3.7) we have⁸

$$\bar{\mathcal{I}}_p(q_T, Q) = q_T \int_0^\infty db b J_0(bq_T) \ln^p \left(\frac{bQ}{b_0} \right), \quad (\text{C.1})$$

where $b_0 = 2 \exp(-\gamma_E)$. These integrals may be evaluated from

$$\bar{\mathcal{I}}_p(q_T, Q) = \frac{d^p}{du^p} \bar{\mathcal{I}}(q_T, Q; u)|_{u=0} \quad (\text{C.2})$$

where

$$\begin{aligned} \bar{\mathcal{I}}(q_T, Q) &= q_T \int_0^\infty db b J_0(bq_T) \left(\frac{bQ}{b_0} \right)^u \\ &= -\frac{2e^{u\gamma_E}}{\pi q_T} \left(\frac{Q}{q_T} \right)^u \sin \left(\frac{\pi u}{2} \right) \Gamma^2 \left(1 + \frac{u}{2} \right), \end{aligned} \quad (\text{C.3})$$

which can be written as

$$\begin{aligned} \bar{\mathcal{I}}(q_T, Q) &= -\frac{ue^{u\gamma_E}}{q_T} \left(\frac{Q}{q_T} \right)^u \frac{\Gamma(1+u/2)}{\Gamma(1-u/2)} \\ &= -\frac{u}{q_T} \left(\frac{Q}{q_T} \right)^u \exp \left[-2 \sum_{k=1}^{\infty} \frac{\zeta_{2k+1}}{2k+1} \left(\frac{u}{2} \right)^{2k+1} \right]. \end{aligned} \quad (\text{C.4})$$

This gives instead of Eq. (3.13)

$$\begin{aligned} \bar{\mathcal{I}}_1(q_T, Q) &= -\frac{1}{q_T}, \quad \bar{\mathcal{I}}_2(q_T, Q) = -\frac{2}{q_T} \ln \left(\frac{Q}{q_T} \right) \\ \bar{\mathcal{I}}_3(q_T, Q) &= -\frac{3}{q_T} \ln^2 \left(\frac{Q}{q_T} \right) \\ \bar{\mathcal{I}}_4(q_T, Q) &= -\frac{4}{q_T} \left[\ln^3 \left(\frac{Q}{q_T} \right) - \frac{1}{2} \zeta_3 \right]. \end{aligned} \quad (\text{C.5})$$

Therefore at small $q_T > 0$ we expect

$$\left[\frac{q_T}{\sigma_0^H} \frac{d\sigma_H}{dq_T} \right]_{\text{NLO}} \sim a_R (\bar{G}_0 R_0 + \bar{G}'_1 R'_1) + a_R^2 (\bar{H}_0 R_0 + \bar{H}_1 R_1 + \bar{H}'_1 R'_1 + \bar{H}'_2 R'_2 + \bar{H}''_2 R''_2) \quad (\text{C.6})$$

where, writing $L = \ln(Q/q_T)$,

$$\begin{aligned} \bar{G}_0 &= \bar{H}_1 = 4A_g^{(1)}L + 2B_g^{(1)}, \quad \bar{G}'_1 = -1, \\ \bar{H}_0 &= 4L \left[A_g^{(2)} + \beta_0 B_g^{(1)} - \beta_0 A_g^{(1)} \ln \left(\frac{Q^2}{\mu_R^2} \right) \right] + 8\beta_0 A_g^{(1)} L^2 \\ &\quad + 2 \left[\bar{B}_g^{(2)} - \beta_0 B_g^{(1)} \ln \left(\frac{Q^2}{\mu_R^2} \right) \right] - 8(A_g^{(1)})^2 \left(L^3 - \frac{1}{2} \zeta_3 \right) \\ &\quad - 12A_g^{(1)} B_g^{(1)} L^2 - 4(B_g^{(1)})^2 L, \\ \bar{H}'_1 &= 6A_g^{(1)} L^2 + 4B_g^{(1)} L, \\ \bar{H}'_2 &= -1, \quad \bar{H}''_2 = -2L. \end{aligned} \quad (\text{C.7})$$

⁸Here we ignore the shift in the argument of the logarithm, which gives only power corrections.

Here we have allowed for the possibility that the coefficient $\overline{B}_g^{(2)}$ for q_T may be different from $B_g^{(2)}$ for E_T . Comparing with Eqs. (3.14) and (3.15), we see that the NLO E_T and q_T distributions at the point $q_T = E_T$ differ by

$$\left. \frac{d\sigma_H}{dE_T} - \frac{d\sigma_H}{dq_T} \right|_{q_T=E_T} \sim a_R^2 \frac{\sigma_B^H}{E_T} \left[H_0 - \overline{H}_0 + (H'_1 - \overline{H}'_1) \frac{R'_1}{R_0} \right] \quad (\text{C.8})$$

where $\sigma_B^H = \sigma_0^H R_0$ is the Born cross section and

$$\begin{aligned} H_0 - \overline{H}_0 &= \frac{4}{3} \pi^2 A_g^{(1)} \left(2A_g^{(1)} L + B_g^{(1)} \right) + 2 \left(B_g^{(2)} - \overline{B}_g^{(2)} \right) + 12\zeta_3 \left(A_g^{(1)} \right)^2, \\ H'_1 - \overline{H}'_1 &= -\frac{2}{3} \pi^2 A_g^{(1)}. \end{aligned} \quad (\text{C.9})$$

D. Alternative Monte Carlo results

For purposes of comparison with alternative descriptions of the parton shower, hadronization and the underlying event, we provide here results equivalent to those obtained using `Herwig++` in Sec. 4, using the `Pythia8` event generator [35, 36]. We use the default parameters appearing in `Pythia8` version 8.185, with the Higgs boson mass set to 126 GeV. Figure 11 is equivalent to Fig. 6 for `Herwig++` and demonstrates that the reweighting procedure reproduces the analytical resummed and matched result.

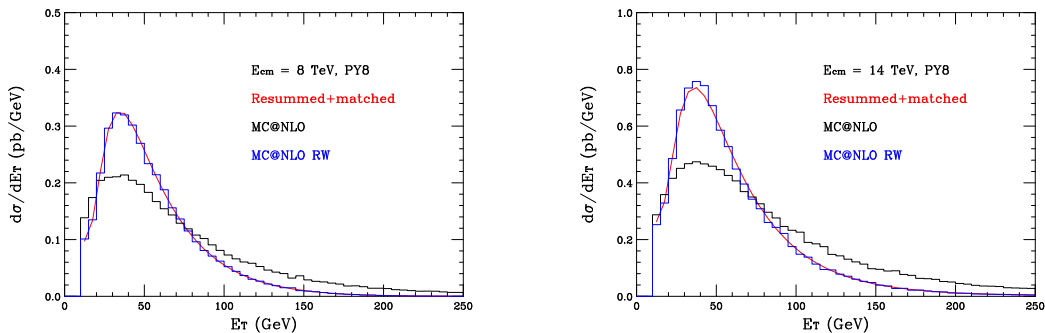


Figure 11: Parton-level transverse-energy distribution in Higgs boson production at the LHC at 8 and 14 TeV. Red: resummed and matched to NLO. Black: `aMC@NLO+Pythia8` before reweighting. Blue: `aMC@NLO+Pythia8` after reweighting.

In Fig. 12 we show the effect of hadronization on the parton-level E_T distribution. Comparing to Fig. 9, it can be observed that the effect is of similar magnitude and the compensation obtained by applying a cut of $|\eta| < 5$ persists in `Pythia8`.

The effect of the underlying event model present in `Pythia8` is shown in Fig. 13. Evidently, the effect is qualitatively similar to what was shown in Fig. 10 for `Herwig++`. Moreover, the effect of imposing a minimum transverse momentum on the contributing hadrons is also identical to that observed in `Herwig++`.

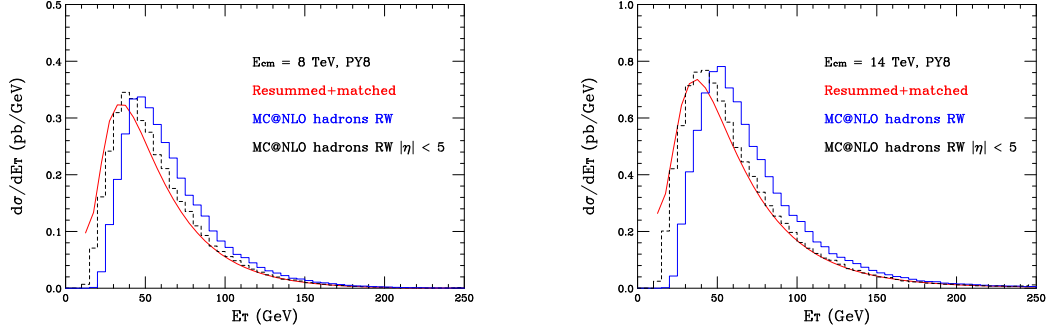


Figure 12: Hadron-level transverse-energy distribution in Higgs boson production at the LHC at 8 and 14 TeV. Red: resummed and matched to NLO. Blue: aMC@NLO+Pythia8. Black dashes: aMC@NLO+Pythia8 particles restricted to lie within pseudorapidity $|\eta| < 5$.

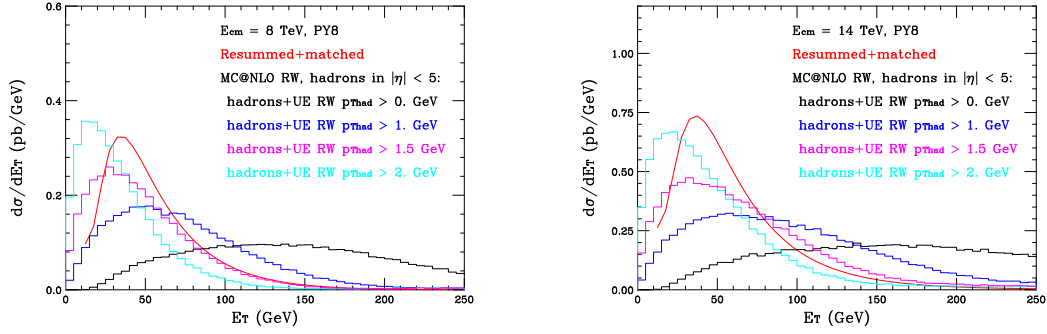


Figure 13: Hadron-level transverse-energy distribution in Higgs boson production at the LHC at 8 and 14 TeV, including the effect of the underlying event. Red: resummed and matched to NLO. aMC@NLO+Pythia8 events with hadron maximum pseudorapidity $\eta^c = 5$: Black: $p_T^c = 0$ GeV, Blue: $p_T^c = 1.0$ GeV, Magenta: $p_T^c = 1.5$ GeV, Cyan: $p_T^c = 2.0$ GeV.

References

- [1] G. Aad *et al.* [ATLAS Collaboration], Phys. Lett. B **716** (2012) 1 [arXiv:1207.7214 [hep-ex]].
- [2] S. Chatrchyan *et al.* [CMS Collaboration], Phys. Lett. B **716** (2012) 30 [arXiv:1207.7235 [hep-ex]].
- [3] A. Papaefstathiou, J. M. Smillie and B. R. Webber, JHEP **1004** (2010) 084 [arXiv:1002.4375 [hep-ph]].
- [4] F. Halzen, A. D. Martin, D. M. Scott and M. P. Tuite, Z. Phys. C **14** (1982) 351.
- [5] C. T. H. Davies and B. R. Webber, Z. Phys. C **24** (1984) 133.
- [6] G. Altarelli, G. Martinelli and F. Rapuano, Z. Phys. C **32** (1986) 369.

- [7] G. Parisi and R. Petronzio, Nucl. Phys. B154 (1979) 427.
- [8] J. C. Collins, D. E. Soper and G. Sterman, Nucl. Phys. B **250** (1985) 199.
- [9] G. Bozzi, S. Catani, G. Ferrera, D. de Florian and M. Grazzini, Phys. Lett. B **696** (2011) 207 [arXiv:1007.2351 [hep-ph]].
- [10] T. Becher and M. Neubert, Eur. Phys. J. C **71** (2011) 1665 [arXiv:1007.4005 [hep-ph]].
- [11] G. Bozzi, S. Catani, D. de Florian and M. Grazzini, Nucl. Phys. B **737** (2006) 73 [hep-ph/0508068].
- [12] G. Bozzi, S. Catani, D. de Florian and M. Grazzini, Nucl. Phys. B **791** (2008) 1 [arXiv:0705.3887 [hep-ph]].
- [13] S. Mantry and F. Petriello, Phys. Rev. D **81** (2010) 093007 [arXiv:0911.4135 [hep-ph]].
- [14] S. Catani and M. Grazzini, Nucl. Phys. B **845** (2011) 297 [arXiv:1011.3918 [hep-ph]].
- [15] A. Banfi, G. P. Salam and G. Zanderighi, JHEP **1206** (2012) 159 [arXiv:1203.5773 [hep-ph]].
- [16] T. Becher and M. Neubert, JHEP **1207** (2012) 108 [arXiv:1205.3806 [hep-ph]].
- [17] A. Banfi, P. F. Monni, G. P. Salam and G. Zanderighi, Phys. Rev. Lett. **109** (2012) 202001 [arXiv:1206.4998 [hep-ph]].
- [18] T. Becher, M. Neubert and L. Rothen, JHEP **1310** (2013) 125 [arXiv:1307.0025 [hep-ph]].
- [19] I. W. Stewart, F. J. Tackmann, J. R. Walsh and S. Zuberi, arXiv:1307.1808.
- [20] S. Catani, D. de Florian and M. Grazzini, Nucl. Phys. B **596**, 299 (2001) [arXiv:hep-ph/0008184].
- [21] S. Catani, E. D’Emilio and L. Trentadue, Phys. Lett. B211 (1988) 335.
- [22] R. P. Kauffman, Phys. Rev. D45 (1992) 1512.
- [23] D. de Florian and M. Grazzini, Phys. Rev. Lett. **85** (2000) 4678 [arXiv:hep-ph/0008152].
- [24] D. de Florian and M. Grazzini, Nucl. Phys. B **616** (2001) 247 [arXiv:hep-ph/0108273].
- [25] S. Frixione, P. Nason and G. Ridolfi, Nucl. Phys. B **542** (1999) 311 [hep-ph/9809367].
- [26] D. de Florian and M. Grazzini, Nucl. Phys. B **704** (2005) 387 [hep-ph/0407241].
- [27] A. D. Martin, W. J. Stirling, R. S. Thorne and G. Watt, Eur. Phys. J. C **63** (2009) 189 [arXiv:0901.0002 [hep-ph]].
- [28] S. Catani and M. Grazzini, Phys. Rev. Lett. **98** (2007) 222002 [hep-ph/0703012].
- [29] M. Grazzini, JHEP **0802** (2008) 043 [arXiv:0801.3232 [hep-ph]].
- [30] S. Catani and M. Grazzini, Eur. Phys. J. C **72** (2012) 2013 [Erratum-ibid. C **72** (2012) 2132] [arXiv:1106.4652 [hep-ph]].
- [31] M. Bahr *et al.*, Eur. Phys. J. C **58** (2008) 639 [arXiv:0803.0883 [hep-ph]]; arXiv:0812.0529 [hep-ph]. <http://projects.hepforge.org/herwig/>
- [32] K. Arnold, L. d’Errico, S. Gieseke, D. Grellscheid, K. Hamilton, A. Papaefstathiou, S. Platzer and P. Richardson *et al.*, arXiv:1205.4902 [hep-ph].
- [33] S. Frixione and B. R. Webber, JHEP **0206** (2002) 029 [hep-ph/0204244].

- [34] R. Frederix, S. Frixione, V. Hirschi, F. Maltoni, R. Pittau and P. Torrielli, *JHEP* **1202** (2012) 099 [arXiv:1110.4738 [hep-ph]].
- [35] T. Sjostrand, S. Mrenna and P. Z. Skands, *JHEP* **0605** (2006) 026 [hep-ph/0603175].
- [36] T. Sjostrand, S. Mrenna and P. Z. Skands, *Comput. Phys. Commun.* **178** (2008) 852 [arXiv:0710.3820 [hep-ph]].
- [37] D. de Florian, G. Ferrera, M. Grazzini and D. Tommasini, *JHEP* **1111** (2011) 064 [arXiv:1109.2109 [hep-ph]].
- [38] L. Durand and H. Pi, *Phys. Rev. D* **40** (1989) 1436.
- [39] J. M. Butterworth, J. R. Forshaw and M. H. Seymour, *Z. Phys. C* **72** (1996) 637 [arXiv:hep-ph/9601371]. <http://projects.hepforge.org/jimmy/>
- [40] I. Borozan and M. H. Seymour, *JHEP* **0209** (2002) 015 [hep-ph/0207283].
- [41] S. Gieseke, C. Rohr and A. Siodmok, *Eur. Phys. J. C* **72** (2012) 2225 [arXiv:1206.0041 [hep-ph]].
- [42] A. Sherstnev and R. S. Thorne, *Eur. Phys. J. C* **55** (2008) 553 [arXiv:0711.2473 [hep-ph]]; arXiv:0807.2132 [hep-ph].
- [43] M. R. Whalley, D. Bourilkov and R. C. Group, hep-ph/0508110.
- [44] The ATLAS collaboration, ATLAS-CONF-2013-072.